

structure can be taken into account thanks to the design of dedicated kernels where the structure drives the combination of the feature information [SSvL⁺11, NAK16, VSKB10a]. When dealing with time series, Dynamic Time Warping and related approaches are based on the similarity between the features while allowing temporal distortion in the time instants that are matched. These approaches have many applications for time series classification or clustering and lead to state-of-the-art results on several benchmarks [CB17, SC78]. For image classification, Segmentation Graph Kernels [BH07] aim to emphasize image structure while respecting pixels distribution resulting on a graph kernel for images. However, no generic framework for the comparison of structured objects has been proposed yet.

On the other hand, distributions or probability measures are meaningful representations for data in machine learning. Optimal Transport (OT) distances provide an elegant way of comparing distributions by capturing the underlying geometric property through a cost function. With long standing applications in computer graphics and vision (e.g. [RTG00, RPDB12]), OT has started to receive a lot of attention in the machine learning community (e.g. [HGK⁺16, CFTR17, ACB17, SCSJ17]). Yet, the natural formulation of OT cannot leverage the structural information of objects since it only relies on a cost function that compares their feature representations.

However, some modifications over OT formulation have been made in order to compare structural information of objects. Following the pioneering work by Mémoli [Mem11], Peyré *et al.* [PCS16a] propose a way of comparing two distance matrices that can be seen as representations of some objects structures. They use an OT metric called Gromov-Wasserstein distance capable of comparing two metric spaces even if they do not lie in the same ground space and apply it to compute barycenter of molecular shapes. Even though this approach has wide applications, it only encodes the intrinsic structural information in the transportation problem. To the best of our knowledge, the problem of including both structural and feature information in a unified OT formulation remains largely under-addressed.

OT distances that include both features and structures Recent approaches tend to incorporate the structure information as a regularization of the OT problem. For example in [AMJJ18] and [CFTR17] authors constrain transport maps to favor some assignments in certain groups. These approaches require a known and simple structure such as class clusters to work but do not generalize well to more general structural information. In their work [TPK⁺17], Thorpe *et al.* propose an OT distance that combines both a Lagrangian formulation of a signal and its temporal structural information. They define a metric, called Transportation L^p distance, that can be seen as a distance over the coupled space of time and feature. They apply it for signal analysis and show that combining both structure and feature tends to better capture the signal information. Yet, for their approach to work, the structure and feature information should lie in the same ambient space, which is not a valid assumption for more general problems such as similarity between graphs.

Contributions We propose a new framework capable of taking into account both structural and feature information into the optimal transport problem. The framework can compare any usual structured machine learning data even if the feature and structural information dwell in spaces of different dimensions (e.g. compact of \mathbb{R}^n and \mathbb{R}^m with $n \neq m$), which cannot be done by any other OT method. We define a new distance with metric properties that can be efficiently computed for both the quadratic program case and its entropy regularized counterpart. Moreover the importance of the structure and feature information can be adjusted by a trade-off parameter. After recalling basic notions on OT (Section 2), we describe our new distance and detail its properties, along with computational solutions (Section 3). In the experiments (Section 4), we show its application to graph classification and barycenter computation.

Notations Let (Ω, d) be a measurable metric space. The simplex histogram with N bins will be denoted as $\Sigma_N = \{a \in (\mathbb{R}_+^*)^N, \sum_i a_i = 1, \}$. For two histograms $a \in \Sigma_n$ and $b \in \Sigma_m$ we note $\Pi(a, b)$ the set of all couplings of a and b , i.e. the set $\Pi(a, b) = \{\pi \in \mathbb{R}_+^{n \times m} \mid \sum_i \pi_{i,j} = b_j; \sum_j \pi_{i,j} = a_i\}$. We also note \otimes the tensor product, i.e. for a tensor $L = (L_{i,j,k,l})$, $L \otimes B$ is the matrix $\left(\sum_{k,l} L_{i,j,k,l} B_{k,l}\right)_{i,j}$ and $\langle \cdot \rangle$ the matrix scalar product associated with the Frobenius norm. For $x \in \Omega$, δ_x denotes the dirac in x .

2 Background on OT distances

We consider a discrete setting where a structured object is described by a graph G in which each vertex of the graph is associated with a feature vector. As described in the introduction this setting encompasses a wide range of structured machine learning objects. G is described by $(\{x_i, v_i\})_{i \in [1, \dots, n]}$ where $X = (x_1, \dots, x_n) \in \Omega^n$ is the set of features and $V = (v_1, \dots, v_n)$ the set of the graph vertices. To this extent, features x_i are structured by the intrinsic relation between the vertices v_i . With such a depiction, the object can be described by a joint discrete probability measure $\mu = \sum_{i=1}^n a_i \delta_{(x_i, v_i)}$, where $a = (a_1, \dots, a_n)$ aims to adjust the significance of each vertex.

Structured data space Previous description leads to consider a structured data as an element of set $H(\Omega) = \bigcup_{n \in \mathbb{N}, s} H_n^s(\Omega)$ where $H_n^s(\Omega) \stackrel{def}{=} \{\mu = \sum_{i=1}^n a_i \delta_{(x_i, v_i)}; a \in \Sigma_n; x_i \in \Omega; v_i \in \Omega_s\}$ where $(\Omega_s)_s$ are measurable metric spaces. This set includes all graphs with any number of vertices (from Ω_s), where each vertex v_i is associated to a feature x_i in Ω and a weight a_i on the simplex. For instance on segmented images, one can take the graph as the spatial neighborhood of the segmented zones, the features as the average color in the zone, and the weights as the ratio of image pixels in the zone.

Wasserstein distance The p -Wasserstein distance (also known as Earth Mover’s distance [RTG00] when $p = 1$) between two discrete probability measures $\gamma = \sum_{i=1}^n a_i \delta_{x_i}$ and $\beta = \sum_{j=1}^m b_j \delta_{y_j}$ is :

$$\mathcal{W}_p(\gamma, \beta) = \left(\min_{\pi \in \Pi(a, b)} \langle \pi, M_{XY}^p \rangle \right)^{\frac{1}{p}} \quad (1)$$

where $M_{XY} = (d(x_i, y_j))_{i, j}$ the $n \times m$ distance matrix between elements. This quantity is nul *iff* $\gamma = \beta$ and in this case features match exactly. The p -Wasserstein distance has a nice geometrical interpretation as it represents the optimal cost *w.r.t.* the ground space distance in order to “move” the probability measure γ onto β with $\pi(i, j)$ the amount of probability mass shifted from x_i to y_j . Computing this distance involves solving a linear program which can be done with supercubical complexity. Yet, a version with entropic regularization can be computed with quadratic complexity [Cut13, AWR17]. Despite many desirable properties, the Wasserstein distance can only compare probability measures as long as their supports live in the same ground space Ω , failing to compare two probability measures with supports on spaces with different dimensions.

Gromov-Wasserstein distance On the other hand, another OT distance allows the comparison of distributions that do not necessarily live in the same ambient space. By relaxing the classical Hausdorff distance [Vil08] that is untractable in practice, [Stu06, MS04] build a distance over “the space of spaces”, called the Gromov-Wasserstein distance, by comparing the intrinsic distances in each space. Considering $\rho = \sum_i a_i \delta_{v_i}$ and $\theta = \sum_j b_j \delta_{w_j}$ with v_i and w_j in different metric spaces Ω_{s_1} and Ω_{s_2} and $C_1(i, k)$ a distance or similarity between v_i and v_k (in the same way C_2 for the w_j), we introduce the 4 dimensional tensor $L(C_1, C_2)$:

$$L_{i, j, k, l}(C_1, C_2) = |C_1(i, k) - C_2(j, l)|$$

measuring the similarity between all pair-to-pair distances. To compute the Gromov-Wasserstein distance one must solve :

$$\mathcal{GW}_p(C_1, C_2, \rho, \theta) = \left(\min_{\pi \in \Pi(a, b)} \sum_{i, j, k, l} L_{i, j, k, l}(C_1, C_2)^p \pi_{i, j} \pi_{k, l} \right)^{\frac{1}{p}} = \left(\min_{\pi \in \Pi(a, b)} \langle L(C_1, C_2)^p \otimes \pi, \pi \rangle \right)^{\frac{1}{p}}.$$

Computing the Gromov-Wasserstein distance requires solving a quadratic program which can be computationally expensive when done by classical solver. However, [PCS16b] proposes an efficient algorithm based on entropy regularization. The resulting coupling tends to associate pairs of points with similar distances within each pair: the more similar $C_1(i, k)$ is to $C_2(j, l)$ the stronger the transport coefficients $\pi_{i, j}$ and $\pi_{k, l}$ will be. The main property of the Gromov-Wasserstein distance is that it defines a metric over the space of all metric spaces quotiented by measure-preserving isometries (see [MS04]). Informally, “shapes” and “sizes” of objects compared by the Gromov-Wasserstein distance are equivalent if the distance is nul, allowing the comparison of measures over different ground spaces.

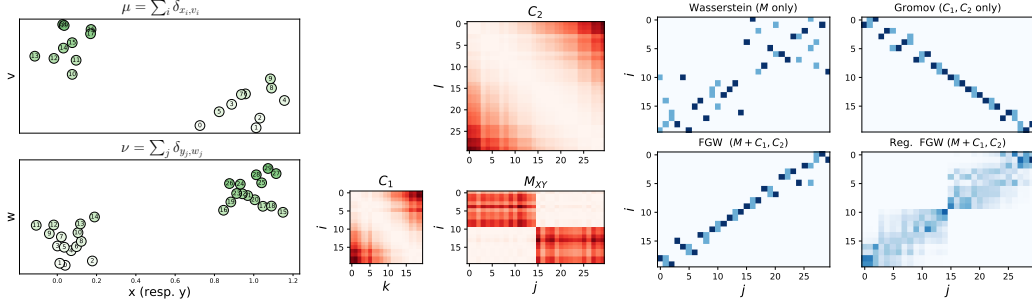


Figure 1: Illustration of the difference between \mathcal{W} , \mathcal{GW} and \mathcal{FGW} couplings. (left) empirical distributions μ with 20 samples and ν with 30 samples which color is proportional to their index. (middle) Cost matrices in the feature (M_{XY}) and structure domains (C_1, C_2) with similar samples in white. (right) Solution for all methods. Dark blue indicates a non zero coefficient of the transportation map between i and j . Feature distances is large between points laying on the diagonal of $M_{X,Y}$ such that Wasserstein maps is anti-diagonal but unstructured. Fused Gromov-Wasserstein incorporates both feature and structure maps in a single transport map.

3 Fused Gromov-Wasserstein approach for structured data

3.1 Fused Gromov-Wasserstein distance (FGW)

Building on both Wasserstein and Gromov-Wasserstein distances, we define in this paper a new distance dedicated to structured data, viewed as the combination of a structural information and a feature information. In the next paragraphs, $\mu \in H_n^1(\Omega)$ and $\nu \in H_m^2(\Omega)$ are structured data as described in the previous part. We suppose $n \geq m$. C_1 and C_2 are the distance matrices inherent to each graph, and x_i, y_j the features in each node, L is a similarity measure over \mathbb{R} and $p, q \geq 1$.

Using previous notations, we propose a novel Optimal Transport discrepancy called the Fused Gromov-Wasserstein distance and defined as:

$$\mathcal{FGW}_{p,q,\alpha}(C_1, C_2, \mu, \nu) = \left(\min_{\pi \in \Pi(a,b)} E_{p,q}(M_{XY}, C_1, C_2, \pi) \right)^{\frac{1}{p}} \quad (2)$$

where:

$$E_{p,q}(M_{XY}, C_1, C_2, \pi) = \sum_{i,j,k,l} (d(x_i, y_j)^q + \alpha L[C_1(i, k), C_2(j, l)]^q)^p \pi_{i,j} \pi_{k,l}$$

With this definition, the resulting coupling π is computed with respect to the structure and the features. Note that the optimal coupling tends to associate pairs of feature and structure points with similar distances within each structure pair and with similar features. α allows a trade-off between the relative importance of the feature and the structural information. Figure 1 illustrates the differences between Wasserstein, Gromov-Wasserstein and Fused Gromov-Wasserstein couplings π^* .

Theorem 3.1. \mathcal{FGW} defines a metric for $q = 1$ and a semi-metric for $q > 1$

If $L = |\cdot|$, $q = 1$, and C_1, C_2 are distance matrices then \mathcal{FGW} defines a metric over $H(\Omega)$ quotiented by the measure preserving isometries that are also feature preserving. More precisely, \mathcal{FGW} satisfies the triangle inequality and is nul iff there exists an application $\sigma : \{1, \dots, n\} \rightarrow \{1, \dots, m\}$ such that :

$$b_j = \sum_{i \in \sigma^{-1}(j)} a_i \quad (3)$$

$$\forall i \in \{1, \dots, n\}, x_i = y_{\sigma(i)} \quad (4)$$

$$\forall i, j \in \{1, \dots, n\} \times \{1, \dots, n\}, C_1(i, j) = C_2(\sigma(i), \sigma(j)) \quad (5)$$

If $q > 1$, the triangle inequality is relaxed by a factor 2^{q-1} such that \mathcal{FGW} defines a semi-metric over $H(\Omega)$

All proofs can be found in the supplementary materials. The resulting application σ preserves the importance of each node (eq (10)), of the features (eq (11)) and the two objects structure (eq (12)).

The metric \mathcal{FGW} can be used in a wide set of applications such as k -nearest-neighbors, distance-substitution kernels, pseudo-Euclidean embeddings, or representative-set methods. Arguably, such a distance allows for interpretation of the similarity (with the optimal mapping π), contrary to end-to-end learning machines such as neural networks.

3.2 Fused Gromov-Wasserstein barycenter

An interesting use of the \mathcal{FGW} distance is to define a barycenter of a set of structured data as a Fréchet mean. In that context, we look for the structured data that minimizes the sum of the (weighted) \mathcal{FGW} distances within a given set of objects. OT barycenters have many desirable properties and applications [AC11, PCS16b], yet no formulation can leverage both structural and feature information in the barycenter computation. Here we propose using \mathcal{FGW} distance to compute the barycenter of structured data $(\mu_k)_k \in H(\Omega)^k$ associated with structures $(C_k)_k$, features $(Y_k)_k$ and base histograms $(a_k)_k$. We suppose that the feature space is $\Omega = (\mathbb{R}^d, l_2)$ and $p = 1$. For simplicity, we assume that the base histograms and the histogram a associated to the barycenter are known and fixed.

In this context, for a fixed $N \in \mathbb{N}$ and $(\lambda_k)_k$ such that $\sum_k \lambda_k = 1$, we aim to find:

$$\min_{C \in \mathbb{R}^{N \times N}, \mu} \sum_k \lambda_k \mathcal{FGW}_{1,q,\alpha}(C, C_k, \mu, \mu_k) = \min_{C, X \in \mathbb{R}^{N \times d}, (\pi_k)_k} \sum_k \lambda_k E_{1,q}(M_{XY_k}, C, C_k, \pi_k) \quad (6)$$

Note that this problem is convex *w.r.t* C and X but not *w.r.t* π_k . We discuss the proposed algorithm to solve this problem in the next section. Intuitively, looking for a barycenter means finding feature values supported on a fixed size support, and the structure that relates them. Interestingly enough, there are several variants of this problem, where features or structure can be fixed for the barycenter. Solving the related simpler optimization problem extends straightforwardly. We give examples of this both in the experimental section and supplemental material.

3.3 Optimization and algorithmic solution

In this section we discuss the numerical optimization problem for computing the \mathcal{FGW} distance between discrete distributions with the case $p = 1$ (the general case $p > 1$ easily derives from the next discussion).

Solving the Quadratic Optimization problem Equation 2 is clearly a quadratic problem *w.r.t.* π . Note that despite the apparent $\mathcal{O}(m^2n^2)$ complexity of computing the tensor product, one can simplify the sum to complexity $\mathcal{O}(mn^2 + m^2n)$ with Eq. 7 when considering $q = 2$. In this case, the \mathcal{FGW} computation problem can be re-written as finding π^* such that:

$$\pi^* = \arg \min_{\pi \in \Pi(a,b)} \text{vec}(\pi)^T Q \text{vec}(\pi) + \text{vec}(M)^T \text{vec}(\pi) \quad (7)$$

where $Q = -2\alpha C_2 \otimes_K C_1$, \otimes_K denotes the Kronecker product of two matrices, and vec the column-stacking operator. With such form, the resulting optimal map can be seen as a quadratic regularized map from initial Wasserstein problem similarly to [DPR16]. However, unlike this approach, we have a quadratic but non necessarily convex term to the initial problem. The gradient G that arises from Eq. (2) can be expressed with the following partial derivative *w.r.t.* π :

$$G = M_{XY}^q + 2\alpha L(C_1, C_2)^q \otimes \pi \quad (8)$$

that can be computed with $\mathcal{O}(mn^2 + m^2n)$ operations when $q = 2$.

Solving a large scale QP with a classical solver can be computationally expensive. In [FPPA14], authors propose a solver for a graph regularized optimal transport problem whose resulting optimization problem is also a QP. We can then directly use their conditional gradient defined in Alg. 1 to solve our optimization problem. It only needs at each iteration to compute the gradient in Eq. (8) and to solve a classical OT problem for instance with a network flow algorithm. While the problem is non convex, conditional gradient is known to converge to a local stationary point [LJ16].

Solving the Regularized QP When entropic regularization is used [PCS16b], the optimization problem computes $\mathcal{FGW}^\lambda = E_{p,q}(M_{XY}, C_1, C_2, \pi_\lambda^*)$ by finding π_λ^* such that:

$$\pi_\lambda^* = \underset{\pi \in \Pi(a,b)}{\text{argmin}} E_{p,q}(M_{XY}, C_1, C_2, \pi) + \lambda H(\pi) \quad (9)$$

Algorithm 1 Conditional Gradient (CG) for FGW

```

1:  $\pi^{(0)} \leftarrow \mu_X \mu_Y^\top$ 
2: for  $i = 1, \dots, \mathbf{do}$ 
3:    $G \leftarrow$  Gradient from Eq. (8) w.r.t.  $\pi^{(i-1)}$ 
4:    $\tilde{\pi}^{(i)} \leftarrow$  Solve OT with ground loss  $G$ 
5:    $\tau^{(i)} \leftarrow$  Line-search for loss (2) with  $\tau \in (0, 1)$ 
6:    $\pi^{(i)} \leftarrow (1 - \tau^{(i)})\pi^{(i-1)} + \tau^{(i)}\tilde{\pi}^{(i)}$ 
7: end for

```

Algorithm 2 Projected gradient for regularized FGW

```

1:  $\pi^{(0)} \leftarrow \mu_X \mu_Y^\top$ 
2: for  $i = 1, \dots, \mathbf{do}$ 
3:    $G \leftarrow$  Gradient from Eq. (8) w.r.t.  $\pi^{(i-1)}$ 
4:    $\pi^{(i)} \leftarrow$  Solve Sinkhorn with loss  $G$  and reg.  $\lambda$ 
5: end for

```

where $H(\pi) = \sum_{i,j} \pi_{i,j} (\log(\pi_{i,j}) - 1)$ and $\lambda > 0$ is the regularization parameter. Entropic regularization is used in order to speed up the computation of the initial solution in Eq. (2). However, note that the resulting minimum does not lead to a distance anymore (the distance between an object and itself is no longer equal to zero). Following the same scheme as the Sinkhorn Loss (Theorem (1) in [GPC17]) we rather compute for (μ, C_1) and (ν, C_2) the normalized similarity measure $\mathcal{FGW}_{p,q,\alpha}^\lambda(C_1, C_2, \mu, \nu) = 2\mathcal{FGW}_{p,q,\alpha}^\lambda(C_1, C_2, \mu, \nu) - \mathcal{FGW}_{p,q,\alpha}^\lambda(C_1, C_1, \mu, \mu) - \mathcal{FGW}_{p,q,\alpha}^\lambda(C_2, C_2, \nu, \nu)$. [PCS16b] propose an efficient algorithm based on Bregman projections to solve the Gromov-Wasserstein optimization problem. Their approach relies on a projected gradient algorithm for which each iteration is performed by solving an efficient Sinkhorn-Knopp matrix scaling [Cut13]. This approach can be very easily adapted to our problem by using the gradient in Eq. (8) instead of the gradient for only the quadratic term as in standard Gromov-Wasserstein (See Alg. 2).

One limit of the projected gradient discussed above is that the gradient step is fixed as $1/\lambda$ which means that either the problem is solved quickly with large regularization but converges very slowly, or we can have a larger step at the risk of encountering numerical stability problems.

Solving the barycenter problem with Block Coordinate Descent (BCD) We propose to minimize (7) using a BCD algorithm, *i.e.* iteratively minimizing with respect to the couplings π_k , to the metric C and the feature vector X . The minimization of this problem *w.r.t.* $(\pi_k)_k$ is equivalent to compute S independent Fused Gromov-Wasserstein distances as discussed above. We consider $L = |\cdot|$, and $q = 2$. Minimization *w.r.t.* C in this case has a closed form (see Prop. 4 in [PCS16b]) :

$$C \leftarrow \frac{1}{aa^T} \sum_k \lambda_k \pi_k^T C_k \pi_k$$

Minimization *w.r.t.* X can be computed with $X \leftarrow \sum_k \lambda_k Y_k \pi_k^T \text{diag}(\frac{1}{a})$ (see eq (8) in [CD14]).

4 Experimental results

We now illustrate the behaviour of \mathcal{FGW} on synthetic and real datasets. The algorithms presented in the previous section have been implemented using Python Optimal Transport toolbox [FC17].

4.1 Illustration of \mathcal{FGW} on trees

We construct two trees as illustrated in Figure 2 where the 1D node features are shown with colors (in red, features belong to $[0, 1]$ and in blue in $[9, 10]$). The structure similarity matrices C_1 and C_2 are the shortest path between nodes. Figure 2 illustrates the behavior of regularized \mathcal{FGW} distance when trade-off parameter α changes. The left part recovers the Wasserstein distance ($\alpha = 0$): red nodes are transported on red ones and the blue nodes on the blue ones. For a strong alpha (right), we recover the Gromov-Wasserstein distance: all couples of points are transported to another couple of points, without taking into account the features. Finally, for an intermediate α (center), the bottom and first level structure is preserved as well as the feature matching (red on red and blue on blue).

4.2 Graph-structured data classification

Datasets We consider 6 widely used benchmark datasets. MUTAG [DLdCD⁺91], PTC-MR [KGW16], NCI1 [WWK08] are graphs derived from small molecules, PROTEINS and ENZYMES [BK05] represent macromolecules and IMDB-B, IMDB-M [YV15] are derived from social networks.

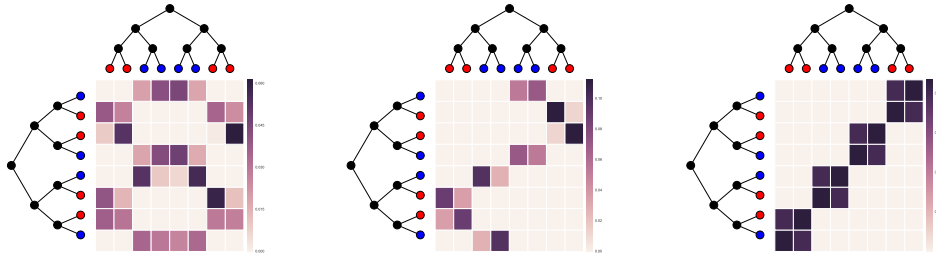


Figure 2: Difference on transportation maps between FGW and W distances on synthetic trees for different values of alpha. On the left $\alpha=0$, on the middle α is intermediate and on the right α is strong.

Table 1: Classification accuracies on the graph datasets. Best results are boldfaced; second best are underlined.

DATASET	LABELED GRAPHS			SOCIAL GRAPHS		VECTOR ATTRIBUTES GRAPH	
	MUTAG	PTC	NCI1	IMDB-B	IMDB-M	PROTEIN	ENZYMES
WL	80.72±3.0	56.97±2.0	80.22±0.5	-	-	72.9±0.5	53.7±1.4
GK	81.58±2.1	57.32±1.1	43.89±0.4	65.87±0.98	43.89±0.38	62.28±0.29	-
RW	83.68±1.66	57.26±1.30	-	-	-	74.22±0.42	-
SP	85.79±2.51	58.53±2.55	73.00±0.51	-	-	75.07±0.54	-
WL-OA	84.5±1.7	63.6±1.5	86.1±0.2	-	-	76.4±0.4	59.9±1.1
PSCN $k = 10$	88.95±4.37	62.29±5.62	76.34±1.68	71.00±2.29	45.23±2.84	75.00±2.51	-
FGW CG	86.8±5.4	58.3±8.4	78.7±1.9	66.4±3.6	48.5±3.0	76.0±1.9	66.3±6.5
FGW SINK	81.6±5.9	56.9±6.6	75.3±2.3	70.6±2.8	45.5±2.8	77.0±4.0	55.5±5.1

All data can be found in [KKM⁺16]. MUTAG, PTC, NCI1 have labeled node attributes, PROTEIN and ENZYMES have vector node attributes.

Experimental setup The \mathcal{FGW} distance is computed by considering the feature distance matrix M_{XY} between node features as following: if features are discrete labels, we consider the dirac distance between them, if nodes have real attributes we consider the l_2 distance. Structure distances C_1 and C_2 are whether the shortest path between nodes or the weighted shortest path [Che11] if nodes have real attributes. We calculate the regularized \mathcal{FGW} with Bregman projection as in Alg. 2. We consider the kernel $e^{-\gamma \mathcal{FGW}}$, where $\gamma \geq 0$ is chosen by cross validation. Note that this kernel is not positive definite, and we regularize non-positive definite kernel shifting eigenvalue such that every eigenvalue turns positive. For each dataset we perform 10 folds cross-validation with LIBSVM, using 9 folds for training and 1 for testing, and we repeat the experiments 10 times. We compare our results with state-of-the-art graph kernel methods and CNN on graphs (PSCN) from [NAK16] and report also results for WL-OA graph kernel using [KGW16], in which the experimental setup is the same. (SP) denotes the shortest path kernel [BK05], (RW) the random walk kernel [GFW03], (WL) the Weisfeler Lehman Kernel [VSKB10b], (GK) the graphlet count kernel [SVP⁺09], (WL-OA) the Weisfeler Optimal Assignment Kernel [KGW16] and (PSCN) the PATCHY-SAN framework with hyperparameter k leading to most accurate scores on average (see [NAK16]). We report average prediction accuracies and standard deviations for all methods in Table 1. Non reported results indicate that the accuracy score for the method is not available in the corresponding publication.

Results and discussion In these experiments, the case $\alpha = 0$ was never chosen during validation, showing the benefit of our approach over simple Wasserstein distance between nodes. In some cases, regularization improves the score but in much cases it tends to degrade overall performances. Indeed in many situations the Bregman projection algorithm for solving regularized \mathcal{FGW} faced instability so “high” regularization parameter λ had to be chosen in order to converge to a solution: this might have led to over-regularized solutions where graphs are indistinguishable. However even if the classification approach relies on a simple eigenvalue shifting on the non-PSD kernel, the accuracy scores are most of the times better than dedicated graph-kernel based state-of-the-art methods. Hence we believe that the \mathcal{FGW} distance is well suited for emphasizing the structure and the feature information of an object. The interesting part is that the design of appropriate metrics C_1 and C_2 can be flexible regarding the problem. For example, in the case of PROTEIN and ENZYMES datasets where real attributes are available, using the weighted shortest path leads to better results than shortest path matrices.

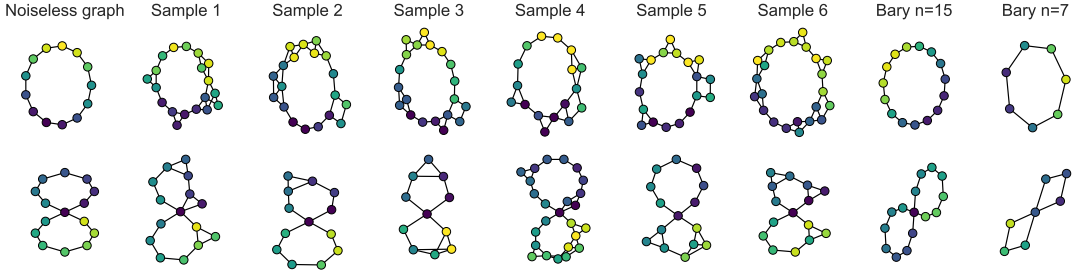


Figure 3: Illustration of \mathcal{FGW} graph barycenter. The first column illustrates the original settings with the denoised graphs, and columns 2 to 7 are noisy samples that constitute the datasets. Columns 8 and 9 show the barycenters for each setting, with different number of nodes. Blue nodes indicates a feature value close to -1 , yellow nodes close to 1 .

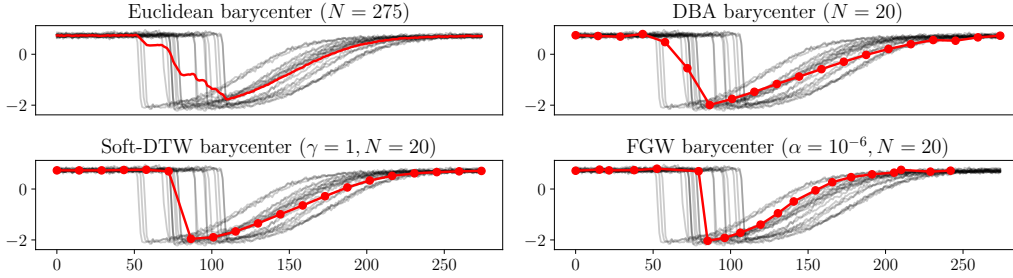


Figure 4: Time series barycenters for one class of the Trace dataset.

4.3 Barycenters for structured data

Graph barycenter In this experiment, we use \mathcal{FGW} to compute barycenters of toy graphs. We generate graphs following either a circle or ∞ symbol with 1D features following a sine and linear variation respectively. The number of nodes is drawn randomly between 10 and 25 and some noise is added to the features and to the structure (some connections with the third neighbors are randomly added). We compute the \mathcal{FGW} barycenter containing 10 samples using the shortest path distance between the nodes as the structural information and the ℓ_2 distance for the features. We recover an adjacency matrix by thresholding the similarity matrix C given by the barycenter. Results are showed in Figure 3. One major benefit of the barycenter is its capability of denoising and compressing. Hence the structure is conserved and the features follow the same law as the original. Moreover we can compress the information by selecting a number of nodes that compose the barycenter, which remains denoised. To the best of our knowledge no other method can compute such graphs barycenters.

Time series barycenter We now consider the computation of \mathcal{FGW} barycenters in the time series context. Considered time series correspond to one class of the *Trace* dataset from the UEA archive [BLVK]. We compute short barycenters (20 time instants) and compare our results with both DBA [PKG11] and soft-DTW [CB17] in Figure 4. We consider the ℓ_2 distance between the timestamps as the structural information, and the same to compute the distance between the features. Timestamps of the \mathcal{FGW} barycenter are retrieved (up to a time shift) through MDS on the barycentric structure matrix C . DTW-based approaches are fully invariant to local time distortions, failing to capture the good “shape” of the time series, whereas the obtained \mathcal{FGW} barycenter successfully follows the natural pace in the signal, which is especially visible on the second half of the times series. Most importantly, \mathcal{FGW} allows the generation of an irregularly sampled barycenter, hence focusing on highly informational parts of the time series.

5 Discussion and conclusion

We have presented in this work a new class of distances based on optimal transport that allows comparisons between structured objects. It considers those objects as probability measures defined over two feature and structural spaces that are connected together. A coupling is sought that tries to match them optimally with respect to a pairing cost between features and structures. We theoretically

prove that it defines indeed a distance on structured data, allowing us to consider geometrical objects such as barycenters. We provide algorithmic solutions for its computation, illustrate its versatility in handling several types of structured objects and show its efficiency on the graph classification problem, where it reaches and sometimes surpasses the state-of-the-art performances. We believe that this metric can have a significant impact on challenging graph signal analysis problems. Current work under examination deals with the continuous counterpart of those distances and their mathematical properties. Also, applications of this metric as a loss in structured deep learning architectures (e.g. deep auto-encoders) will be considered.

References

- [AC11] Martial Agueh and Guillaume Carlier. Barycenters in the wasserstein space. *SIAM Journal on Mathematical Analysis*, 43(2):904–924, 2011.
- [ACB17] M. Arjovsky, S. Chintala, and L. Bottou. Wasserstein generative adversarial networks. In *Proceedings of the 34th International Conference on Machine Learning*, volume 70, pages 214–223, Sydney, Australia, 06–11 Aug 2017.
- [ACOL00] Marc Alexa, Daniel Cohen-Or, and David Levin. As-rigid-as-possible shape interpolation. In *Proceedings of the 27th annual conference on Computer graphics and interactive techniques*, pages 157–164. ACM Press/Addison-Wesley Publishing Co., 2000.
- [AMJJ18] David Alvarez-Melis, Tommi S. Jaakkola, and Stefanie Jegelka. Structured Optimal Transport. In *AISTATS*, 2018.
- [AWR17] Jason Altschuler, Jonathan Weed, and Philippe Rigollet. Near-linear time approximation algorithms for optimal transport via sinkhorn iteration. In *Advances in Neural Information Processing Systems*, pages 1961–1971, 2017.
- [BH07] F. Bach and Z. Harchaoui. Image classification with segmentation graph kernels. In *CVPR*, volume 00, pages 1–8, 06 2007.
- [BHS⁺07] Gükhan H. Bakir, Thomas Hofmann, Bernhard Schölkopf, Alexander J. Smola, Ben Taskar, and S. V. N. Vishwanathan. *Predicting Structured Data (Neural Information Processing)*. The MIT Press, 2007.
- [BK05] Karsten M. Borgwardt and Hans-Peter Kriegel. Shortest-path kernels on graphs. In *ICDM, ICDM '05*, pages 74–81, Washington, DC, USA, 2005. IEEE Computer Society.
- [BLVK] Antony Bagnall, Jason Lines, Williams Vickers, and Eamonn Keogh. The uea & ucr time series classification repository. www.timeseriesclassification.com.
- [CB17] Marco Cuturi and Mathieu Blondel. Soft-DTW: a differentiable loss function for time-series. In *Proceedings of the ICML*, volume 70, pages 894–903, International Convention Centre, Sydney, Australia, 06–11 Aug 2017. PMLR.
- [CD14] Marco Cuturi and Arnaud Doucet. Fast computation of wasserstein barycenters. In Eric P. Xing and Tony Jebara, editors, *Proceedings of the 31st International Conference on Machine Learning*, volume 32 of *Proceedings of Machine Learning Research*, pages 685–693, Beijing, China, 22–24 Jun 2014. PMLR.
- [CFTR17] Nicolas Courty, Rémi Flamary, Devis Tuia, and Alain Rakotomamonjy. Optimal transport for domain adaptation. *IEEE TPAMI*, 39(9):1853–1865, 2017.
- [Che11] Pavel Chebotarev. A class of graph-geodetic distances generalizing the shortest-path and the resistance distances. *Discrete Applied Mathematics*, 159(5):295 – 302, 2011.
- [Cut13] Marco Cuturi. Sinkhorn distances: Lightspeed computation of optimal transport. In *NIPS*, pages 2292–2300, 2013.
- [DLdCD⁺91] Asim Kumar Debnath, Rosa L. Lopez de Compadre, Gargi Debnath, Alan J. Shusterman, and Corwin Hansch. Structure-activity relationship of mutagenic aromatic and heteroaromatic nitro compounds. correlation with molecular orbital energies and hydrophobicity. *Journal of Medicinal Chemistry*, 34(2):786–797, 1991.
- [DPR16] A. Dessein, N. Papadakis, and J.-L. Rouas. Regularized Optimal Transport and the Rot Mover’s Distance. *ArXiv e-prints*, October 2016.

- [FC17] Rémi Flamary and Nicolas Courty. Pot python optimal transport library. 2017.
- [FPPA14] Sira Ferradans, Nicolas Papadakis, Gabriel Peyré, and Jean-François Aujol. Regularized discrete optimal transport. *SIAM Journal on Imaging Sciences*, 7(3):1853–1882, 2014.
- [GFW03] Thomas Gärtner, Peter Flach, and Stefan Wrobel. On graph kernels: Hardness results and efficient alternatives. In *IN: CONFERENCE ON LEARNING THEORY*, pages 129–143, 2003.
- [GPC17] Aude Geneway, Gabriel Peyré, and Marco Cuturi. Learning Generative Models with Sinkhorn Divergences. Working Papers 2017-83, Center for Research in Economics and Statistics, October 2017.
- [HGK⁺16] G. Huang, C. Guo, M. Kusner, Y. Sun, F. Sha, and K. Weinberger. Supervised word mover’s distance. In *Advances in Neural Information Processing Systems*, pages 4862–4870, 2016.
- [KGW16] Nils M. Kriege, Pierre-Louis Giscard, and Richard C. Wilson. On valid optimal assignment kernels and applications to graph classification. *CoRR*, abs/1606.01141, 2016.
- [KKM⁺16] Kristian Kersting, Nils M. Kriege, Christopher Morris, Petra Mutzel, and Marion Neumann. Benchmark data sets for graph kernels, 2016.
- [LJ16] Simon Lacoste-Julien. Convergence rate of frank-wolfe for non-convex objectives. *arXiv preprint arXiv:1607.00345*, 2016.
- [Mem11] Facundo Memoli. Gromov wasserstein distances and the metric approach to object matching. *Foundations of Computational Mathematics*, pages 1–71, 2011. 10.1007/s10208-011-9093-5.
- [MS04] Facundo Mémoli and Guillermo Sapiro. Comparing point clouds. In *Proceedings of the 2004 Eurographics/ACM SIGGRAPH Symposium on Geometry Processing*, SGP ’04, pages 32–40, New York, NY, USA, 2004. ACM.
- [NAK16] Mathias Niepert, Mohamed Ahmed, and Konstantin Kutzkov. Learning convolutional neural networks for graphs. In Maria Florina Balcan and Kilian Q. Weinberger, editors, *ICML*, volume 48 of *Proceedings of Machine Learning Research*, pages 2014–2023, New York, New York, USA, 20–22 Jun 2016. PMLR.
- [PCS16a] Gabriel Peyré, Marco Cuturi, and Justin Solomon. Gromov-Wasserstein Averaging of Kernel and Distance Matrices. In *ICML*, Proc. 33rd ICML, New-York, United States, June 2016.
- [PCS16b] Gabriel Peyré, Marco Cuturi, and Justin Solomon. Gromov-wasserstein averaging of kernel and distance matrices. In *ICML*, pages 2664–2672, 2016.
- [PKG11] François Petitjean, Alain Ketterlin, and Pierre Gançarski. A global averaging method for dynamic time warping, with applications to clustering. *Elsevier Pattern Recognition*, 44(3):678–693, 2011.
- [RPDB12] Julien Rabin, Gabriel Peyré, Julie Delon, and Marc Bernot. Wasserstein barycenter and its application to texture mixing. In Alfred M. Bruckstein, Bart M. ter Haar Romeny, Alexander M. Bronstein, and Michael M. Bronstein, editors, *Scale Space and Variational Methods in Computer Vision*, pages 435–446, Berlin, Heidelberg, 2012. Springer Berlin Heidelberg.
- [RTG00] Yossi Rubner, Carlo Tomasi, and Leonidas J. Guibas. The earth mover’s distance as a metric for image retrieval. *International Journal of Computer Vision*, 40(2):99–121, Nov 2000.
- [SC78] Hiroaki Sakoe and Seibi Chiba. Dynamic programming algorithm optimization for spoken word recognition. *ieeesssp*, 26(1):43–49, 1978.
- [SCSJ17] Matthew Staib, Sebastian Claiici, Justin M Solomon, and Stefanie Jegelka. Parallel streaming wasserstein barycenters. In *Advances in Neural Information Processing Systems*, pages 2644–2655, 2017.
- [SP04] Robert W Sumner and Jovan Popović. Deformation transfer for triangle meshes. In *ACM Transactions on Graphics (TOG)*, volume 23, pages 399–405. ACM, 2004.

- [SSvL⁺11] Nino Shervashidze, Pascal Schweitzer, Erik Jan van Leeuwen, Kurt Mehlhorn, and Karsten M. Borgwardt. Weisfeiler-lehman graph kernels. *J. Mach. Learn. Res.*, 12:2539–2561, November 2011.
- [Stu06] Karl-Theodor Sturm. On the geometry of metric measure spaces. *Acta Mathematica*, 196(1):65–131, Jul 2006.
- [SVP⁺09] Nino Shervashidze, S. V. N. Vishwanathan, Tobias H. Petri, Kurt Mehlhorn, and et al. Efficient graphlet kernels for large graph comparison, 2009.
- [TPK⁺17] Matthew Thorpe, Serim Park, Soheil Kolouri, Gustavo K. Rohde, and Dejan Slepčev. A transportation l^p distance for signal analysis. *Journal of Mathematical Imaging and Vision*, 59(2):187–210, Oct 2017.
- [Vil08] Cédric Villani. *Optimal Transport: Old and New*. Grundlehren der mathematischen Wissenschaften. Springer, 2009 edition, September 2008.
- [VSKB10a] S. V. N. Vishwanathan, Nicol N. Schraudolph, Risi Kondor, and Karsten M. Borgwardt. Graph kernels. *J. Mach. Learn. Res.*, 11:1201–1242, August 2010.
- [VSKB10b] S. V. N. Vishwanathan, Nicol N. Schraudolph, Risi Kondor, and Karsten M. Borgwardt. Graph kernels. *J. Mach. Learn. Res.*, 11:1201–1242, August 2010.
- [WWK08] Nikil Wale, Ian A. Watson, and George Karypis. Comparison of descriptor spaces for chemical compound retrieval and classification. *Knowledge and Information Systems*, 14(3):347–375, Mar 2008.
- [YV15] Pinar Yanardag and S.V.N. Vishwanathan. Deep graph kernels. In ACM, editor, *Proceedings of the 21th ACM SIGKDD International Conference on Knowledge Discovery and Data Mining*, pages 1365–1374, 2015.

6 Supplementary materials

6.1 \mathcal{FGW} is a distance

In all the proof (Ω, d) in a measurable metric space.

Let (x_i, v_i) , $i \in \{1, \dots, n\}$ and (y_j, w_j) $j \in \{1, \dots, m\}$ be two structured objects, with $x_i, y_j \in \Omega^2$. We note $C_1(i, k)$ the distance between vertices v_i and v_k and $C_2(j, l)$ the distance between vertices w_j and w_l . Let also $a \in \Sigma_n$ and $b \in \Sigma_m$ be the weights of each vertex and

$$\mu = \sum_{i=1}^n a_i \delta_{x_i, v_i}$$

$$\nu = \sum_{j=1}^m b_j \delta_{y_j, w_j}$$

the joint discrete probability measures associated with our structured object.

We note :

$$J_q(C_1, C_2, \pi) = \sum_{i,j,k,l} L(C_1(i, k), C_2(j, l))^q \pi_{i,j} \pi_{k,l}$$

$$H_q(\pi) = \sum_{i,j} d(x_i, y_j)^q \pi_{i,j}$$

$$E_{p,q}(C_1, C_2, \pi) = \sum_{i,j,k,l} (d(x_i, y_j)^q + \alpha L(C_1(i, k), C_2(j, l))^q)^p \pi_{i,j} \pi_{k,l}$$

such that

$$\mathcal{FGW}_{p,q,\alpha}(C_1, C_2, \mu, \nu) = \left(\min_{\pi \in \Pi(a,b)} E_{p,q}(C_1, C_2, \pi) \right)^{\frac{1}{p}}$$

Please note that the minimum exists and hence the \mathcal{FGW} distance is well defined since we minimize a continuous function over a compact set of $\mathbb{R}^{n \times m}$.

For the following proofs we suppose that C_1 and C_2 are distances and that $L = |\cdot|$, $n \geq m$. We recall the theorem :

Theorem 6.1. \mathcal{FGW} defines a metric for $q = 1$ and a semi metric for $q > 1$

- If $L = |\cdot|$, $q = 1$, and C_1, C_2 are distance matrices then \mathcal{FGW} defines a metric over $H(\Omega)$ quotiented by the measure preserving isometries that are also feature preserving. More precisely, \mathcal{FGW} respects the triangle inequality and is nul iff there exists an application $\sigma : \{1, \dots, n\} \rightarrow \{1, \dots, m\}$ such that :

$$b_j = \sum_{i \in \sigma^{-1}(j)} a_i \quad (10)$$

$$\forall i \{1, \dots, n\}, x_i = y_{\sigma(i)} \quad (11)$$

$$\forall i, j \in \{1, \dots, n\} \times \{1, \dots, n\}, C_1(i, j) = C_2(\sigma(i), \sigma(j)) \quad (12)$$

- If $q > 1$, the triangle inequality is relaxed by a factor 2^{q-1} such that \mathcal{FGW} defines a semi metric over $H(\Omega)$

We first prove the equality relation for any $q \geq 1$ and we discuss the triangle inequality in the next section.

6.2 Equality relation

Proposition 1. For all $q \geq 1$, $\mathcal{FGW}_{p,q,\alpha}(C_1, C_2, \mu, \nu) = 0$ iff there exists an application $\sigma : \{1, \dots, n\} \rightarrow \{1, \dots, m\}$ which verifies (10), (11) and (12)

Proof. First, let us suppose that such an application exists. Then if we consider the transport map π associated with $i \rightarrow i$ and $j \rightarrow \sigma(i)$. By eq (10) $\pi \in \Pi(a, b)$ and clearly using (11) and (12):

$$E_{p,q}(C_1, C_2, \pi) = \sum_{i,k} (d(x_i, y_{\sigma(i)})^q + \alpha L(C_1(i, k), C_2(\sigma(i), \sigma(k)))^q)^p a_i b_{\sigma(i)} a_k b_{\sigma(k)} = 0$$

We can conclude that $\mathcal{FGW}_{p,q,\alpha}(C_1, C_2, \mu, \nu) = 0$.

Conversly, suppose that $\mathcal{FGW}_{p,q,\alpha}(C_1, C_2, \mu, \nu) = 0$ and $p, q \geq 1$. We define

$$\hat{C}_1(i, k) = \frac{1}{2}C_1(i, k) + \frac{1}{2}d(x_i, x_k)$$

and

$$\hat{C}_2(j, l) = \frac{1}{2}C_2(j, l) + \frac{1}{2}d(y_j, y_l)$$

two distances over $\{(x_i, v_i), i \in \{1, \dots, n\}\}$ and $\{(y_j, w_j), j \in \{1, \dots, m\}\}$. To prove the existence of such map σ we will prove that the Gromov-Wasstein distance $\mathcal{GW}_{qp}(\hat{C}_1, \hat{C}_2, \mu, \nu)$ is nul.

Let $\pi \in \Pi(a, b)$ be any admissible transportation plan. Then for $n \geq 1$, :

$$\begin{aligned} J_n(\hat{C}_1, \hat{C}_2, \pi) &= \sum_{i,j,k,l} L(\hat{C}_1(i, k), \hat{C}_2(j, l))^n \pi_{i,j} \pi_{k,l} \\ &= \sum_{i,j,k,l} \left| \frac{1}{2}(C_1(i, k) - C_2(j, l)) + \frac{1}{2}(d(x_i, x_k) - d(y_j, y_l)) \right|^n \pi_{i,j} \pi_{k,l} \\ &\leq \sum_{i,j,k,l} \frac{1}{2} |C_1(i, k) - C_2(j, l)|^n \pi_{i,j} \pi_{k,l} + \sum_{i,j,k,l} \frac{1}{2} |d(x_i, x_k) - d(y_j, y_l)|^n \pi_{i,j} \pi_{k,l} \end{aligned}$$

by convexity of $t \rightarrow t^n$ and Jensen inequality. We denote the first term (*) and (**) the second term. Combining triangle inequalities $d(x_i, x_k) \leq d(x_i, y_j) + d(y_j, x_k)$ and $d(y_j, x_k) \leq d(y_j, y_l) + d(y_l, x_k)$ we have :

$$d(x_i, x_k) \leq d(x_i, y_j) + d(x_k, y_l) + d(y_j, y_l) \quad (13)$$

We split (**) in two parts $S_1 = \{i, j, k, l ; d(x_i, x_k) - d(y_j, y_l) \geq 0\}$ and $S_2 = \{i, j, k, l ; d(x_i, x_k) - d(y_j, y_l) \leq 0\}$ such that

$$(**) = \sum_{i,j,k,l \in S_1} (d(x_i, x_k) - d(y_j, y_l))^n \pi_{i,j} \pi_{k,l} + \sum_{i,j,k,l \in S_2} (d(y_j, y_l) - d(x_i, x_k))^n \pi_{i,j} \pi_{k,l}$$

In the same way as eq (13) we have :

$$d(y_j, y_l) \leq d(x_i, x_k) + d(x_i, y_j) + d(x_k, y_l) \quad (14)$$

So eq (13) and (14) :

$$(**) \leq \sum_{i,j,k,l} \frac{1}{2} |d(x_i, y_j) + d(x_k, y_l)|^n \pi_{i,j} \pi_{k,l} \stackrel{def}{=} M_n(\pi)$$

We have shown that :

$$\forall \pi \in \Pi(a, b), \forall n \geq 1, J_n(\hat{C}_1, \hat{C}_2, \pi) \leq \frac{1}{2} J_n(C_1, C_2, \pi) + M_n(\pi) \quad (15)$$

Now let π_* be the optimal coupling for $\mathcal{FGW}_{p,q,\alpha}(C_1, C_2, \mu, \nu)$. If $\mathcal{FGW}_{p,q,\alpha}(C_1, C_2, \mu, \nu) = 0$ then since $E_{p,q}(C_1, C_2, \pi) \geq \alpha^p J_{qp}(C_1, C_2, \pi)$ and $E_{p,q}(C_1, C_2, \pi) \geq H_{qp}(\pi)$:

$$J_{qp}(C_1, C_2, \pi_*) = 0$$

and

$$H_{qp}(\pi_*) = 0$$

Then $\sum_{i,j} d(x_i, y_j)^{qp} \pi_{i,j}^* = 0$. Since all terms are positive we can conclude that $\forall m \in \mathbb{N}^*, \sum_{i,j} d(x_i, y_j)^m \pi_{i,j}^* = 0$. In this way :

$$M_{qp}(\pi^*) = \frac{1}{2} \sum_h \binom{qp}{h} \left(\sum_{i,j} d(x_i, y_j)^h \pi_{i,j}^* \right) \left(\sum_{k,l} d(x_k, y_l)^{qp-h} \pi_{k,l}^* \right) = 0$$

Using eq (15) we have shown :

$$J_{qp}(\hat{C}_1, \hat{C}_2, \pi_*) = 0$$

So π_* is the optimal coupling for $\mathcal{GW}_{qp}(\hat{C}_1, \hat{C}_2, \mu, \nu)$ and $\mathcal{GW}_{qp}(\hat{C}_1, \hat{C}_2, \mu, \nu) = 0$. Thanks to Gromov-Wasserstein properties (see [MS04]) there exists $\sigma : \{1, \dots, n\} \rightarrow \{1, \dots, m\}$ which verifies eq (10) and

$$\forall i, j \in \{1, \dots, n\} \times \{1, \dots, n\}, \hat{C}_1(i, j) = \hat{C}_2(\sigma(i), \sigma(j)) \quad (16)$$

Moreover since π_* is the optimal coupling for $\mathcal{GW}_{qp}(\hat{C}_1, \hat{C}_2, \mu, \nu)$ leading to a cost nul, then π_* is supported by σ , in particular π_* is associated with $i \rightarrow i$ and $j \rightarrow \sigma(i)$. So $H_{qp}(\pi^*) = \sum_i d(x_i, y_{\sigma(i)})^{qp} a_i b_{\sigma(i)}$. Since $H_{qp}(\pi^*) = 0$ and all the weights are strictly positive we can conclude that $x_i = y_{\sigma(i)}$.

In this way, $d(x_i, x_k) = d(y_{\sigma(i)}, y_{\sigma(k)})$, so using the equality (16) we can conclude that

$$\forall i, j \in \{1, \dots, n\} \times \{1, \dots, n\}, C_1(i, j) = C_2(\sigma(i), \sigma(j))$$

□

6.3 Triangle Inequality

Proposition 2. For all $q = 1$, \mathcal{FGW} verifies the triangle inequality.

Proof. To prove the triangle inequality of \mathcal{FGW} distance for arbitrary measures we will use the gluing lemma (see [Vil08]) which stresses the existence of couplings with a prescribed structure. Let $a, b, c \in \Sigma_n \times \Sigma_m \times \Sigma_q$. Let also $\mu = \sum_{i=1}^n a_i \delta_{x_i, v_i}$, $\nu = \sum_{j=1}^m b_j \delta_{y_j, w_j}$ and $\gamma = \sum_{k=1}^q c_k \delta_{z_k, t_k}$ be the associated discrete probability measures, with $x_i, y_j, z_k \in \Omega^3$ and v_i, w_j, t_k the vertices of the associated graphs. We note $C_1(i, k)$ the distance between vertices v_i and v_k , $C_2(i, k)$ the distance between vertices w_i and w_k and $C_3(i, k)$ the distance between vertices t_i and t_k .

Let P and Q be two optimal solutions of the \mathcal{FGW} transportation problem between μ and ν and ν and γ respectively. We define :

$$S = P \text{diag}\left(\frac{1}{b}\right) Q$$

(note that S is well defined since $b_j \neq 0$ for all j). Then by definition $S \in \Pi(a, c) \mathbb{R}_+^{n \times q}$ because :

$$S1_m = P \text{diag}\left(\frac{1}{b}\right) Q1_m = P \text{diag}\left(\frac{1}{b}\right) = P1_m = a \text{ (same reasoning for } c).$$

We first prove the triangle inequality for the case $q = 1$.

By suboptimality of S :

$$\begin{aligned} \mathcal{FGW}_{p,\alpha}(C_1, C_3, \mu, \gamma) &\leq \left(\sum_{i,j} \sum_{k,l} (d(x_i, z_j) + \alpha L(C_1(i, k), C_3(j, l)))^p S_{i,j} S_{k,l} \right)^{\frac{1}{p}} \\ &= \left(\sum_{i,j} \sum_{k,l} (d(x_i, z_j) + \alpha L(C_1(i, k), C_3(j, l)))^p \left(\sum_h \frac{P_{i,h} Q_{h,j}}{b_h} \right) \left(\sum_o \frac{P_{k,o} Q_{o,l}}{b_o} \right) \right)^{\frac{1}{p}} \\ &\leq \left(\sum_{i,j,k,l,h,o} (d(x_i, y_h) + d(y_h, z_j) + \alpha L(C_1(i, k), C_2(h, o)) + \alpha L(C_2(h, o), C_3(j, l)))^p \frac{P_{i,h} Q_{h,j}}{b_h} \frac{P_{k,o} Q_{o,l}}{b_o} \right)^{\frac{1}{p}} \end{aligned}$$

by triangular inequality. We note $F_{i,j,h} = \frac{P_{i,h} Q_{h,j}}{b_h}$. We have using Minkowski inequality:

$$\begin{aligned} \mathcal{FGW}_{p,\alpha}(C_1, C_3, \mu, \gamma) &\leq \left(\sum_{i,j,k,l,h,o} (d(x_i, y_h) + \alpha L(C_1(i, k), C_2(h, o)))^p F_{i,j,h} F_{k,o,l} \right)^{\frac{1}{p}} \\ &+ \left(\sum_{i,j,k,l,h,o} (d(y_h, z_j) + \alpha L(C_2(h, o), C_3(j, l)))^p F_{i,j,h} F_{k,o,l} \right)^{\frac{1}{p}} \end{aligned}$$

Moreover we have :

$$\sum_j \frac{Q_{h,j}}{b_h} = 1, \sum_l \frac{Q_{o,l}}{b_o} = 1, \sum_i \frac{P_{i,h}}{b_h} = 1, \sum_k \frac{P_{k,o}}{b_o} = 1 \quad (17)$$

So,

$$\begin{aligned} \mathcal{FGW}_{p,\alpha}(C_1, C_3, \mu, \gamma) &\leq \left(\sum_{i,j,k,l,h,o} (d(x_i, y_h) + \alpha L(C_1(i, k), C_2(h, o)))^p \frac{P_{i,h} Q_{h,j}}{b_h} \frac{P_{k,o} Q_{o,l}}{b_o} \right)^{\frac{1}{p}} \\ &+ \left(\sum_{i,j,k,l,h,o} (d(y_h, z_j) + \alpha L(C_2(h, o), C_3(j, l)))^p \frac{P_{i,h} Q_{h,j}}{b_h} \frac{P_{k,o} Q_{o,l}}{b_o} \right)^{\frac{1}{p}} \\ &\leq \left(\sum_{i,k,h,o} (d(x_i, y_h) + \alpha L(C_1(i, k), C_2(h, o)))^p P_{i,h} P_{k,o} \right)^{\frac{1}{p}} \\ &+ \left(\sum_{l,j,h,o} (d(y_h, z_j) + \alpha L(C_2(h, o), C_3(j, l)))^p Q_{h,j} Q_{o,l} \right)^{\frac{1}{p}} \end{aligned}$$

Since P and Q are the optimal plans we have :

$$\mathcal{FGW}_{p,\alpha}(C_1, C_3, \mu, \gamma) \leq \mathcal{FGW}_{p,\alpha}(C_1, C_2, \mu, \nu) + \mathcal{FGW}_{p,\alpha}(C_2, C_3, \nu, \gamma)$$

which prove the triangle inequality for $q = 1$. So $\mathcal{FGW}_{p,\alpha}$ defines a metric for $q = 1$

□

Proposition 3. For all $q > 1$, \mathcal{FGW} verifies the relaxed triangle inequality :

$$\mathcal{FGW}_{p,\alpha}(C_1, C_3, \mu, \gamma) \leq 2^{q-1}(\mathcal{FGW}_{p,\alpha}(C_1, C_2, \mu, \nu) + \mathcal{FGW}_{p,\alpha}(C_2, C_3, \nu, \gamma))$$

Proof. Let $q > 1$. Let $\kappa = \frac{1}{2^{q-1}}$. We claim :

$$\forall x, y \in \mathbb{R}_+, (x + y)^q \leq \frac{x^q}{\kappa} + \frac{y^q}{\kappa} \quad (18)$$

Indeed,

$$\begin{aligned} (x + y)^q &= \left(\left(\frac{1}{2^{q-1}} \right)^{\frac{1}{q}} \frac{x}{\left(\frac{1}{2^{q-1}} \right)^{\frac{1}{q}}} + \left(\frac{1}{2^{q-1}} \right)^{\frac{1}{q}} \frac{y}{\left(\frac{1}{2^{q-1}} \right)^{\frac{1}{q}}} \right)^q \leq \left[\left(\frac{1}{2^{q-1}} \right)^{\frac{1}{q-1}} + \left(\frac{1}{2^{q-1}} \right)^{\frac{1}{q-1}} \right]^{q-1} \left(\frac{x^q}{2^{q-1}} + \frac{y^q}{2^{q-1}} \right) \\ &= \frac{x^q}{\frac{1}{2^{q-1}}} + \frac{y^q}{\frac{1}{2^{q-1}}} \end{aligned}$$

Last inequality is a consequence of Hölder inequality. Then using same notations as for the case $q = 1$, we have :

$$\begin{aligned} \mathcal{FGW}_{p,\alpha}(C_1, C_3, \mu, \gamma) &\leq \left(\sum_{i,j} \sum_{k,l} (d(x_i, z_j)^q + \alpha L(C_1(i, k), C_3(j, l))^q)^p S_{i,j} S_{k,l} \right)^{\frac{1}{p}} \\ &= \left(\sum_{i,j} \sum_{k,l} (d(x_i, z_j)^q + \alpha L(C_1(i, k), C_3(j, l))^q)^p \left(\sum_h \frac{P_{i,h} Q_{h,j}}{b_h} \right) \left(\sum_o \frac{P_{k,o} Q_{o,l}}{b_o} \right) \right)^{\frac{1}{p}} \\ &\leq \left(\sum_{i,j,k,l,h,o} \left(\frac{d(x_i, y_h)^q}{\kappa} + \frac{d(y_h, z_j)^q}{\kappa} + \alpha \frac{L(C_1(i, k), C_2(h, o))^q}{\kappa} + \alpha \frac{L(C_2(h, o), C_3(j, l))^q}{\kappa} \right)^p \frac{P_{i,h} Q_{h,j}}{b_h} \frac{P_{k,o} Q_{o,l}}{b_o} \right)^{\frac{1}{p}} \end{aligned}$$

Last inequality is due to eq (18). So using same notations and Minkowski inequality:

$$\begin{aligned} \mathcal{FGW}_{p,\alpha}(C_1, C_3, \mu, \gamma) &\leq \frac{1}{\kappa} \left(\sum_{i,j,k,l,h,o} (d(x_i, y_h)^q + \alpha L(C_1(i, k), C_2(h, o))^q)^p F_{i,j,h} F_{k,o,l} \right)^{\frac{1}{p}} \\ &+ \frac{1}{\kappa} \left(\sum_{i,j,k,l,h,o} (d(y_h, z_j)^q + \alpha L(C_2(h, o), C_3(j, l))^q)^p F_{i,j,h} F_{k,o,l} \right)^{\frac{1}{p}} \end{aligned}$$

Using eq (17) :

$$\begin{aligned} \mathcal{FGW}_{p,\alpha}(C_1, C_3, \mu, \gamma) &\leq \frac{1}{\kappa} \left(\sum_{i,j,k,l,h,o} (d(x_i, y_h)^q + \alpha L(C_1(i, k), C_2(h, o))^q)^p \frac{P_{i,h} Q_{h,j}}{b_h} \frac{P_{k,o} Q_{o,l}}{b_o} \right)^{\frac{1}{p}} \\ &+ \frac{1}{\kappa} \left(\sum_{i,j,k,l,h,o} (d(y_h, z_j)^q + \alpha L(C_2(h, o), C_3(j, l))^q)^p \frac{P_{i,h} Q_{h,j}}{b_h} \frac{P_{k,o} Q_{o,l}}{b_o} \right)^{\frac{1}{p}} \\ &\leq \frac{1}{\kappa} \left(\sum_{i,k,h,o} (d(x_i, y_h)^q + \alpha L(C_1(i, k), C_2(h, o))^q)^p P_{i,h} P_{k,o} \right)^{\frac{1}{p}} \\ &+ \frac{1}{\kappa} \left(\sum_{l,j,h,o} (d(y_h, z_j)^q + \alpha L(C_2(h, o), C_3(j, l))^q)^p Q_{h,j} Q_{o,l} \right)^{\frac{1}{p}} \end{aligned}$$

Since P and Q are the optimal plans we have :

$$\mathcal{FGW}_{p,\alpha}(C_1, C_3, \mu, \gamma) \leq 2^{q-1}(\mathcal{FGW}_{p,\alpha}(C_1, C_2, \mu, \nu) + \mathcal{FGW}_{p,\alpha}(C_2, C_3, \nu, \gamma))$$

Which prove that $\mathcal{FGW}_{p,\alpha}$ defines a semi metric for $q > 1$ with coefficient 2^{q-1} for the triangle inequality relaxation.

□

7 Barycenters on mesh data

We show in this section another example of barycenter. We aim at interpolating between unregistered 3D meshes. We recall that barycenters are expressed as structured objects defined as a weighted mean

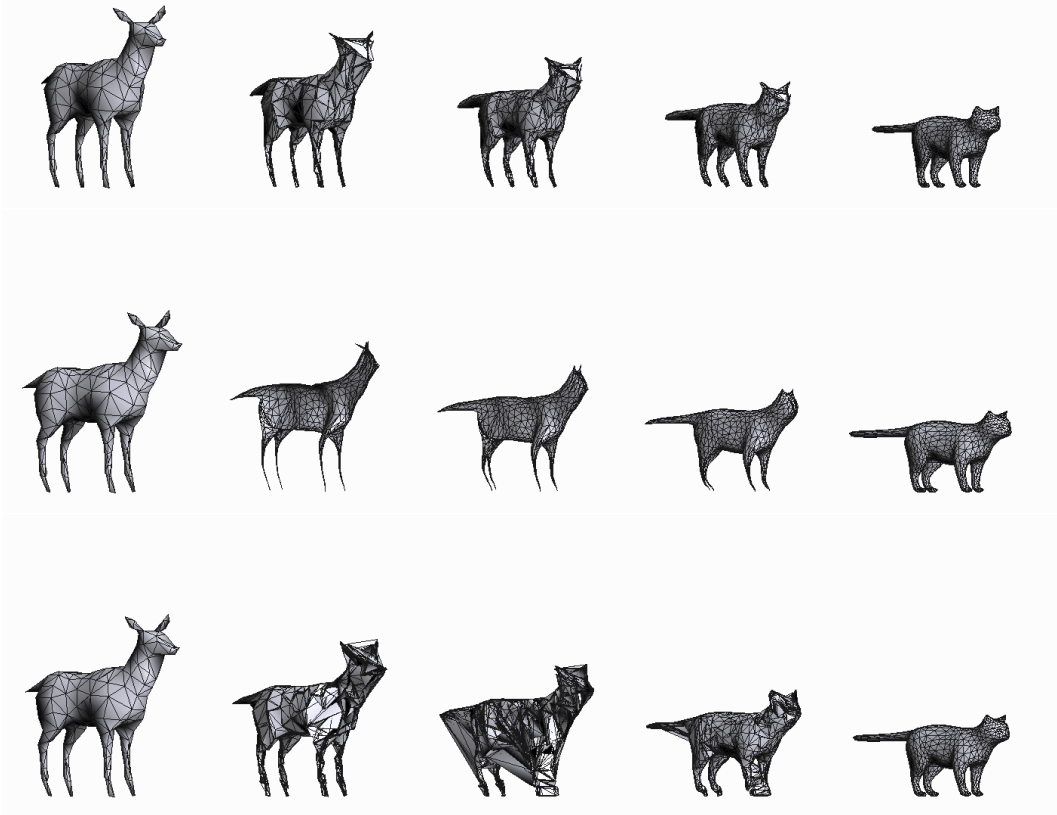


Figure 5: Interpolation of a cat and a deer mesh using \mathcal{FGW} . (first line) interpolation using the non-regularized \mathcal{FGW} distance with a high α value (center line) entropic solution of the same problem (bottomline) same with a very low α value, *i.e.* the mesh structure is almost not taken into account.

of the \mathcal{FGW} distance:

$$\min_{C \in \mathbb{R}^{N \times N}, \mu} \sum_k \lambda_k \mathcal{FGW}_{1,q,\alpha}(C, C_k, \mu, \mu_k) = \min_{C, X \in \mathbb{R}^{N \times d}, (\pi_k)_k} \sum_k \lambda_k E_{1,q}(M_{XY_k}, C, C_k, \pi_k)$$

Here, we consider the problem of interpolating between $k = 2$ 3D meshes that share a common topology but not the same number of vertices. Such an interpolation is realized by setting $\lambda_1 = \lambda$ and $\lambda_2 = 1 - \lambda$ and varying λ between 0 and 1. We interpolate between two quadrupeds: a deer and a cat, that are triangular meshes with respectively 460 and 989 vertices. This is a particularly difficult problem, since no prior correspondences between meshes exist. It has long been considered in the computational geometry and vision communities (e.g. [ACOL00, SP04]), and generally requires user interventions. In our setting, the structure of the barycenter is set to be the one of the cat: the barycenter should have the same topological structure. Our method then only solves for the vertices positions $X \in \mathbb{R}^{989 \times 3}$. The topological structures C_1 and C_2 are set to be the shortest path along the mesh between two vertices, which is a good approximation of the geodesic distance on the manifold.

Results are presented in Figure 7 for $\lambda \in [0.75, 0.5, 0.25]$. A good way of assessing the quality of the results is to visually check that the consistency of the manifold mesh is preserved throughout the interpolation. The first line show the resulting interpolation when the weight on the structure is set to an high value ($\alpha = 10$). When only 3D distances are used to match the shapes (bottom line), one can see that points belonging to different parts of the meshes are matched, because of different densities of points in the two meshes. This results in highly unrealistic mesh. Finally, we also showcase the

effects of using an entropic regularization scheme in our framework (middle line). The regularization strength is set to the minimal possible value that does not yield numerical errors. As vertices are matched with surrounding vertices, and consequently interpolated vertices are convex combinations of more vertices, the mesh tends to shrink. One can though observe that the smoothness of the result is enhanced.